Self-Assembly through Competitive Interactions of Miscible Diblock Copolymer/Homopolymer Blends: Poly(vinylphenol-*b*-methyl methacrylate)/Poly(vinylpyrrolidone) Blend

Wan-Chun Chen,[†] Shiao-Wei Kuo,*[,‡] U-Ser Jeng,[§] and Feng-Chih Chang*[,†]

Institute of Applied Chemistry, National Chiao Tung University, Hsin Chu, Taiwan; Department of Materials and Optoelectronic Engineering, Center for Nanoscience and Nanotechnology, National Sun Yat-Sen University, Kaohsiung, Taiwan; and National Synchrotron Radiation Research Center, Hsinchu Science Park, Taiwan

Received October 1, 2007; Revised Manuscript Received December 6, 2007

ABSTRACT: We have investigated a new type A-*b*-B/C blend system, poly(vinylphenol-*b*-methyl methacrylate)/poly(vinylpyrrolidone) (PVPh-*b*-PMMA)/PVP, where PVPh-*b*-PMMA block (A-*b*-B) copolymer, PVPh/PVP (A/C), and PMMA/PVP (B/C) blends are all miscible through hydrogen bond interaction or dipole−dipole interaction. Because of the significantly stronger hydrogen bond interaction between PVPh and PVP than that between PVPh and PMMA, this miscible PVPh-*b*-PMMA copolymer becomes immiscible up on blending with 20−60 wt % PVP (27−56 wt % PMMA in the blend system) and can self-assemble to form ordered morphologies. Results from small-angle X-ray scattering (SAXS) and TEM consistently indicate that different compositions of PVPh-*b*-PMMA/PVP blends induce different microphase separation structures such as hexagonal and lamellar phases. However, sharp and multiple orders of diffraction are absent from the SAXS profiles, indicating relatively limited sizes of the ordered domains. Large polydispersity in the molecular weight of PVP and small differences in the interaction parameters of the three components of PVPh, PMMA, and PVP are attributed to be the main reasons that limit the microphase separation in this blend system.

Introduction

Blending diblock (A-*b*-B) copolymers with homopolymers have attracted great interest in polymer science during recent decades because of their unusual phase behaviors.[1−28] Most studies have concentrated on an immiscible A-*b*-B diblock copolymer with a homopolymer A.[1−4] Other systems have also been investigated involving blends of homopolymer C with immiscible A-*b*-B diblock copolymer, where C is immiscible with block A but interacts favorably with block B.[7−13] In addition, blend systems comprising an immiscible A-*b*-B diblock copolymer and a homopolymer C, where homopolymer C is miscible with both A and B, have also been investigated by Kwei et al.,[10] as in the blends of poly(styrene-*b*-hydroxystyrene)/poly(vinyl methyl ether) (PS-*b*-PHOST/PVME), where PVME is miscible with both PS and PHOS blocks and can serve as a common solvent in the single phase of a PVME content higher than 50 wt %.

However, A-*b*-B/C systems with all negative but different interaction parameter values of χ_{AB}, χ_{BC}, and χ_{AC} (all binary blends are miscible) have never been reported based on our knowledge. The strong interaction of miscible polymer blends provides great interest in polymer science due to economic incentives arising from their potential applications in thermal, mechanical, and barrier properties.[29−31] Because of the inherent flexible and long-chain nature of most synthetic polymers, specific interactions in polymer blends usually occur in an uncontrollable way and consequently lead to irregular structures.[32] Therefore, it has been a great challenge to construct regular self-assembly structures through specific interactions from polymeric building blocks in bulk state. When all three binary pairs (B/A, B/C, and A/C) are individually miscible in a ternary polymer blend system, a closed immiscibility loop phase separation diagram has been observed.[33] This phenomenon is caused by the difference in the interaction energies among these binary systems, "$\Delta\chi$" and "ΔK" effects in ternary polymer blends such as PVPh/PVAc/PEO,[34] SAA/PMMA/PEO,[35] and phenolic/PEO/PCL[36] systems. Nonetheless, these ternary blend systems only show irregular macroscopic phase separation; a regular self-assembly structure has rarely been observed. A miscible diblock copolymer adopted in this study blending with a third homopolymer tends to confine the phase separation at nanometer scale.

Our previous study showed that PVPh-*b*-PMMA copolymers are fully miscible induced by hydrogen-bonding interactions between the carbonyl groups of PMMA and the hydroxyl groups of PVPh.[37] In addition, both PVP/PMMA and PVPh/PVP blends are all miscible through dipole−dipole and hydrogen-bonding interactions, respectively.[29,44] In this paper, we investigate blends of PVPh-*b*-PMMA diblock copolymer with poly(vinylpyrrolidone) (PVP) homopolymer where the hydrogen-bonding strength is different between PVPh/PVP and PVPh/PMMA blends. On the basis of the Painter−Coleman association model,[38] the interassociation equilibrium constant of the PVPh/PVP blend ($K_A = 6000$)[39] is significantly greater than that of the PVPh-*b*-PMMA block copolymer ($K_A = 47.1$),[37] implying that the hydrogen-bonding interaction between PVPh and PVP is significantly stronger than that between PVPh and PMMA. The homopolymer C is able to form significantly stronger hydrogen-bonding interactions with A block than B block ($\xi_{AC} \gg \xi_{AB}$). In other words, the hydrogen-bonding interactions between PVPh and PVP dominate over that between PVPh and PMMA in PVPh-*b*-PMMA/PVP blends. As a result, the PMMA block tends to be excluded and forms regular self-assembly structures from the PVPh/PVP mixing rich phase.

* To whom correspondence should be addressed: e-mail changfc@mail.nctu.edu.tw; Tel 886-3-5131512; Fax 886-3-5131512. E-mail: kuosw@faculty.nsysu.edu.tw; Tel 886-7-5252000-4079; Fax 886-7-5254099.
[†] National Chiao Tung University.
[‡] National Sun Yat-Sen University.
[§] National Synchrotron Radiation Research Center.

10.1021/ma7021925 CCC: $40.75
Published on Web 01/16/2008

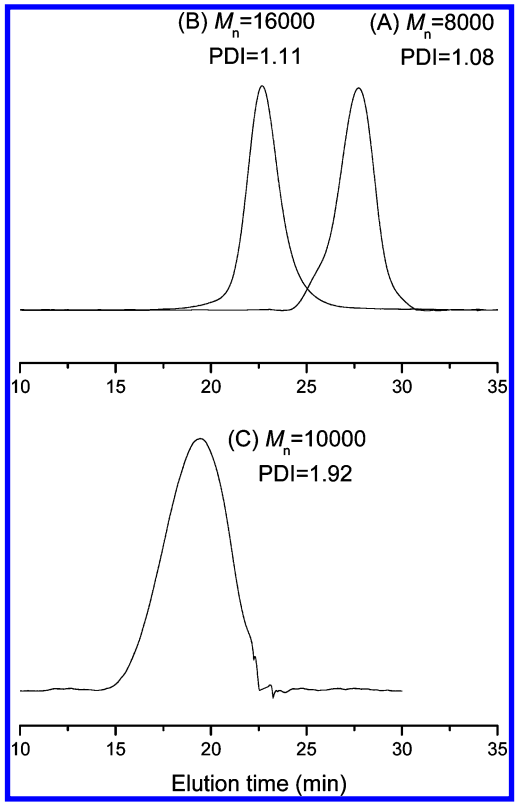

Figure 1. GPC traces of (A) poly(*tert*-butoxystyrene) ($M_w/M_n = 1.08$; $M_n = 8000$ g/mol) and (B) the PVPh-*b*-PMMA block copolymer ($M_w/M_n = 1.11$; $M_n = 16\,000$ g/mol) in THF and (C) poly(vinylpyrrolidone) ($M_w/M_n = 1.92$; $M_n = 10\,000$ g/mol) in DMF.

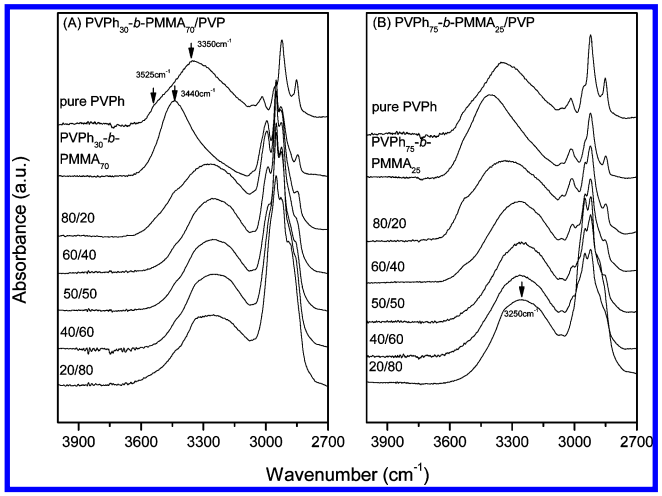

Figure 2. FTIR spectra recorded at 120 °C displaying the hydroxyl stretching vibration region (2700−4000 cm^{-1}) for (A) $PVPh_{30}$-*b*-$PMMA_{70}$/PVP and (B) $PVPh_{75}$-*b*-$PMMA_{25}$/PVP blends with various compositions.

Table 1. Characterization of PVPh-*b*-PMMA Prepared by Anionic Polymerization and PVP

copolymer	M_n	composition of PVPh (wt %)	M_w/M_n
$PVPh_{30}$-*b*-$PMMA_{70}$	16 000	30	1.11
$PVPh_{40}$-*b*-$PMMA_{60}$	16 000	40	1.15
$PVPh_{55}$-*b*-$PMMA_{45}$	30 000	55	1.10
$PVPh_{75}$-*b*-$PMMA_{25}$	22 000	75	1.13
PVP	10 000	0	1.92

Experimental Section

Materials. *N*,*N*′-Dimethylformamide (DMF) (purchased from TEDIA, 99%) was used without further purification. The poly-

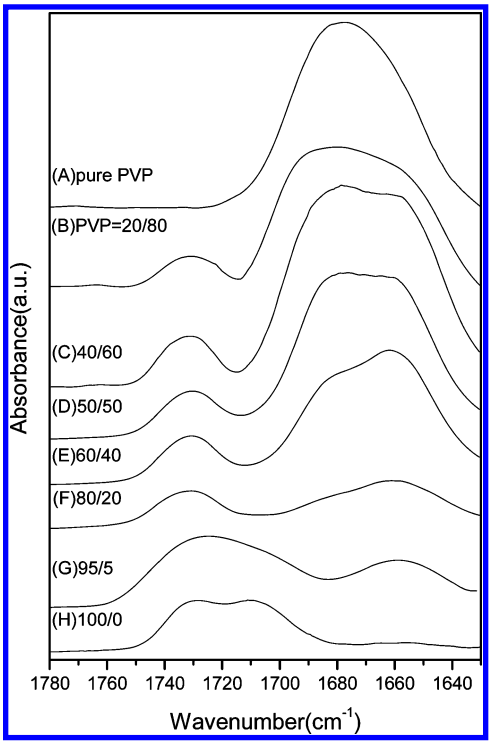

Figure 3. FTIR spectra recorded at 120 °C displaying the carbonyl stretching vibration region (1650−1780 cm^{-1}) for (A) pure PVP and $PVPh_{75}$-*b*-$PMMA_{25}$/PVP blends of various compositions: (B) 20/80, (C) 40/60, (D) 50/50, (E) 60/40, (F) 80/20, (G) 95/5, (H) 100/0 wt %.

(vinylpyrrolidone) (PVP) used in this study was purchased from Aldrich Chemical Co. with a $M_w = 10\,000$. Various PVPh-*b*-PMMA copolymers studied in this work were prepared by living anionic polymerization of 4-*tert*-butoxystyrene and methyl methacrylate, and then the *tert*-butoxy protective group was selectively removed through subsequent hydrolysis reaction as described elsewhere.[37]

Blend Preparation. Blends of various PVPh-*b*-PMMA/PVP compositions were prepared through solution casting. DMF solution containing a 5 wt % polymer mixture was stirred for 6−8 h and then cast on a Teflon dish. The solution was left to evaporate slowly at 80 °C for 1 day and then dried under a vacuum oven at 120 °C for 5 or 14 days for different annealing effect.

Characterizations. The FT-IR spectrum of the KBr disk was measured using a Nicolet Avatar 320 FT-IR spectrometer; 32 scans were collected at a resolution of 1 cm^{-1}. The DMF solution containing the sample was cast onto a KBr disk and dried under conditions similar to those used in the bulk preparation. The sample chamber was purged with nitrogen, and the KBr disk was heated to 120 °C to maintain film dryness. Thermal analysis was carried out using a DSC instrument (DuPont TA 2010). The sample (ca. 5−10 mg) was weighed and sealed in an aluminum pan, quickly cooled to room temperature from the first scan, and then scanned between 30 and 300 °C at a scan rate of 20 °C/min. The glass transition temperature (T_g) was taken as the midpoint of the heat capacity transition between the upper and lower points of deviation from the extrapolated glass and liquid lines. TEM analysis was performed using a Hitachi H-7500 electron microscope operated at 100 kV. Ultrathin sections of the samples were prepared using a Leica Ultracut UCT microtome equipped with a diamond knife. Slices of ca. 700 Å thickness was cut at room temperature. Some of the sliced samples were stained with the vapor from an aqueous solution of RuO_4. The contrast between PMMA and the two other polymers is increased in these samples because PMMA is selectively unstained. Small-angle X-ray scattering (SAXS) experiments were carried out using the SWAXS instrument at the BL17B3 beamline of the National Synchrotron Radiation Research Center (NSRRC), Taiwan.[40] The X-ray beam of 0.5 mm diameter and a wavelength (λ) of 1.24 Å were employed for the SAXS measure-

Table 2. Curve Fitting of the Fraction of Hydrogen-Bonded Carbonyl Groups of $PVPh_{30}$-*b*-$PMMA_{70}$/PVP Blends[a]

	carbonyl group of PMMA							carbonyl group of PVP						
$PVPh_{30}$-*b*-$PMMA_{70}$/PVP	ν_f (cm^{-1})	$W_{1/2}$ (cm^{-1})	A_f (%)	ν_b (cm^{-1})	$W_{1/2}$ (cm^{-1})	A_b (%)	f_b C=O	ν_f (cm^{-1})	$W_{1/2}$ (cm^{-1})	A_f (%)	ν_b (cm^{-1})	$W_{1/2}$ (cm^{-1})	A_b (%)	f_b C=O
100/0	1732	20	67.2	1705	27	32.8	24.6							
95/5	1732	23	80.6	1704	28	19.4	13.9				1662	30	100	100
80/20	1731	23	98.5	1704	28	0.15	1.0	1684	25	23.6	1660	32	76.4	71.4
60/40	1732	21	100				0	1682	25	62.3	1659	31	37.7	31.8
50/50	1732	21	100				0	1682	25	72.3	1658	30	27.7	22.8
40/60	1732	21	100				0	1684	25	79.7	1658	32	20.3	16.4
20/80	1732	21	100				0	1685	26	86.7	1658	32	13.3	10.5

[a] ν_f = wavenumber of free C=O (cm^{-1}); ν_b = wavenumber of hydrogen-bonded C=O (cm^{-1}); A_f = area fraction of free C=O; A_b = area fraction of hydrogen-bonded C=O; f_b = fraction of hydrogen-bonded C=O.

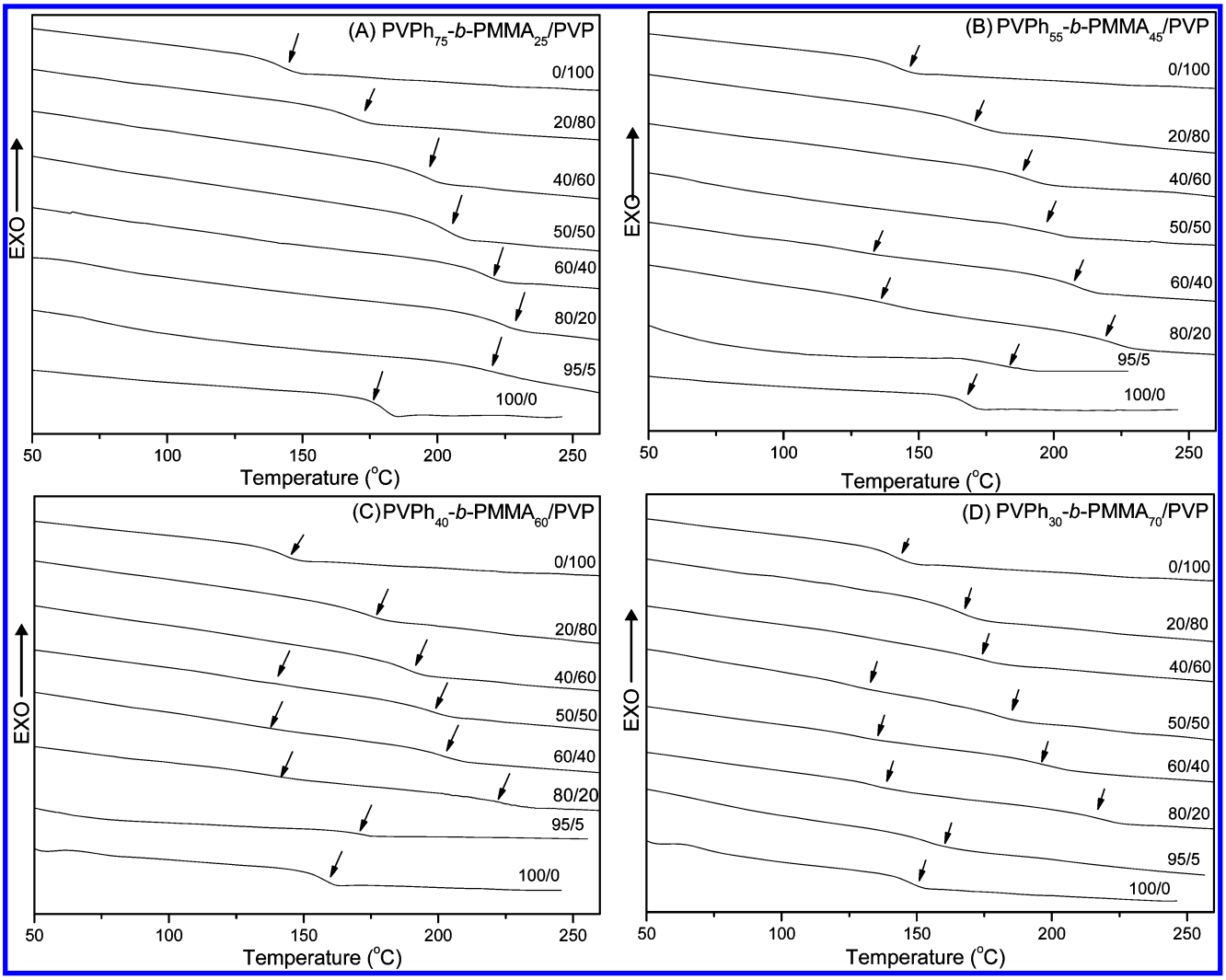

Figure 4. DSC thermograms of PVPh-*b*-PMMA/PVP blends, having different compositions for (A) $PVPh_{75}$-*b*-$PMMA_{25}$/PVP, (B) $PVPh_{55}$-*b*-$PMMA_{45}$/PVP, (C) $PVPh_{40}$-*b*-$PMMA_{60}$/PVP, and (D) $PVPh_{30}$-*b*-$PMMA_{70}$/PVP.

ment. The blending samples of 1 mm thickness in general were sealed between two thin Kapton windows (80 μm in thickness) and measured at room temperature.

Results and Discussion

PVPh-*b*-PMMA copolymers used in this work were prepared by living anionic polymerization as described elsewhere.[37] The GPC traces of a typical PVPh-*b*-PMMA block copolymer obtained after polymerization and hydrolysis are shown in Figure 1, displaying a narrow molecular weight distribution of these diblock copolymers. However, the pure PVP shows relatively higher polydisperstiy (PDI: 1.92) because it was prepared from conventional free radical polymerization. Table 1 summarizes molecular weights of the PVP and several PVPh-*b*-PMMA copolymers employed in this study.

FT-IR Analyses. Infrared spectroscopy has proven to be a powerful tool for investigating specific interactions and the mechanism of interpolymer miscibility through the formation of hydrogen bonds both qualitatively and quantitatively. Several regions within the infrared spectra of PVPh-*b*-PMMA/PVP blends are influenced by the hydrogen-bonding interaction. Figure 2A,B displays the FTIR spectra recorded at 120 °C (to eliminate the moisture absorption influence) in the region of 2700−4000 cm^{-1} (OH stretching) on pure PVPh and various $PVPh_{30}$-*b*-$PMMA_{70}$/PVP and $PVPh_{75}$-*b*-$PMMA_{25}$/PVP blends.

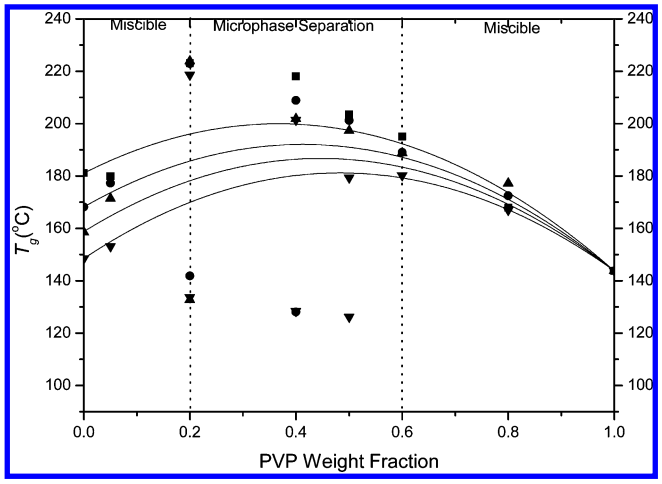

Figure 5. Plots of T_g vs composition curve based on Kwei equation ($k = 1$, $q = 140$) for (■) $PVPh_{75}$-*b*-$PMMA_{25}$/PVP, (●) $PVPh_{55}$-*b*-$PMMA_{45}$/PVP, (▲) $PVPh_{40}$-*b*-$PMMA_{60}$/PVP, and (▼) $PVPh_{30}$-*b*-$PMMA_{70}$/PVP.

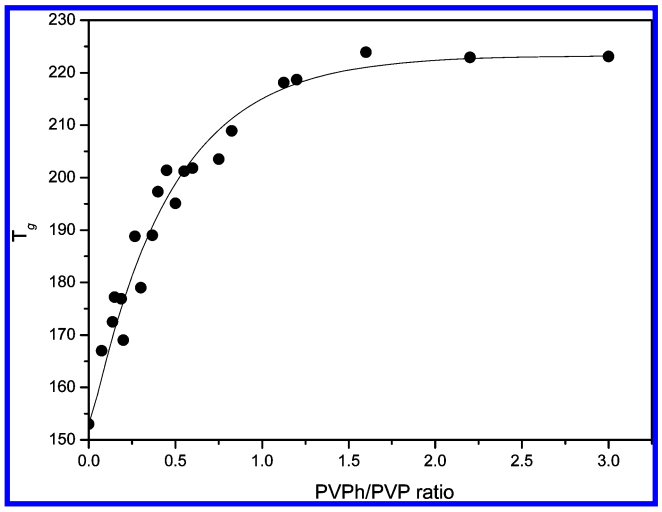

Figure 6. Plots of T_g vs PVPh/PVP ratios.

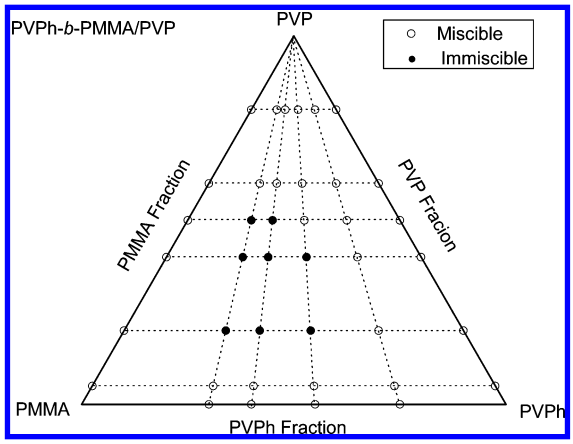

Figure 7. Ternary phase diagram of PVPh-*b*-PMMA/PVP blends.

Under this condition, the pure PVPh shown in Figure 2 is characterized by a very broad band centered at 3350 cm^{-1}, corresponding to the hydrogen-bonded hydroxyl with other hydroxyl as dimer and chainlike multimer. A second narrow band observed at 3525 cm^{-1} as a shoulder is assigned as the free hydroxyl.[29] In addition, for the pure $PVPh_{30}$-*b*-$PMMA_{70}$ copolymer shown in Figure 2A, the broad band representing the self-associated hydroxyl−hydroxyl interaction shifts to higher wavenumber when the PMMA is the rich content in the copolymer. Therefore, it is reasonable to assign the band at 3440 cm^{-1} to the hydrogen-bonded hydroxyl with carbonyl because relatively smaller number of the hydroxyl groups tends to interact completely with carbonyl groups of the PMMA block to form hydrogen bonds. Parts A and B of Figure 2 both display that the hydroxyl shifts into lower wavenumber with the increase of PVP content, implying that PVPh hydroxyl preferably interacts with PVP carbonyl. We assign the band at 3250 cm^{-1} to the hydroxyl interacting with the carbonyl of PVP at higher PVP content. Moskala et al.[41] used the frequency difference ($\Delta\nu$) between the hydrogen-bonded hydroxyl absorption and free hydroxyl absorption to estimate the average strength of the intermolecular interaction. Accordingly, on the basis of the reference of the free hydroxyl stretching at 3525 cm^{-1}, the hydroxyl−carbonyl (PMMA) interassociation ($\Delta\nu = 85$ cm^{-1}) is weaker than the hydroxyl−carbonyl (PVP) interassociation ($\Delta\nu = 275$ cm^{-1}).

Table 3. T_g Behaviors of Various PMMA Weight Percent in PVPh-*b*-PMMA/PVP Blends

PMMA (wt %)	PVPh/PVP (wt %/wt %)	T_g (°C)	
5	15/80	177	
9	11/80	173	
10	30/60	195	
12	8/80	177	
12.5	37.5/50	203	
14	6/80	169	
15	45/40	218	
18	22/60	189	
20	60/20	223	
22.5	27.5/50	201	
24	16/60	188	
27	33/40	208	128
28	12/60	179	126
30	20/50	197	128
36	24/40	223	141
42	18/40	201	128
48	32/20	223	132
56	24/20	218	133
57	38/5	177	
66.5	28.5/5	167	

Figure 3 presents FTIR spectra of the carbonyl stretching region, ranging from 1630 to 1780 cm^{-1}, of pure PVP, PVPh-*b*-PMMA, and their blends at 120 °C. For brevity, we only display the $PVPh_{75}$-*b*-$PMMA_{25}$/PVP blends. Two types of signals for carbonyl stretching appear for the PVPh-*b*-PMMA/PVP blend system: the free and hydrogen-bonded carbonyl stretching bands of PVP (1680 and 1660 cm^{-1}) and PMMA (1730 and 1705 cm^{-1}). The hydrogen-bonded carbonyl stretching band of PMMA at 1705 cm^{-1} vanishes in these blends containing PVP content above 20 wt %, indicating that the PVPh hydroxyl tends to interact with the PVP carbonyl. When the PVPh-*b*-PMMA content is at 20 wt %, the peak at 1660 cm^{-1} corresponding to the hydrogen-bonded carbonyl group of PVP starts to appear as shown in Figure 3F. Here we emphasize that the pure PVP (Figure 3A) shows a relatively broad band of the free carbonyl at 1680 cm^{-1} since the pyrrolidone is able to self-associate strongly through transitional dipole coupling.[39] The Gaussian function has been used to curve fitting the carbonyl stretching frequencies of PVP at 1680 and 1660 cm^{-1} and the PMMA bands at 1730 and 1705 cm^{-1}, corresponding to their respective free and hydrogen-bonded carbonyls. To obtain true fraction of the hydrogen-bonded carbonyl group, a known absorptivity ratio for hydrogen-bonded and free carbonyl is required. Values of $a_{HB}/a_F = 1.5$ for PMMA and 1.3 for PVP are employed,[39] and Table 2 summarizes all of these curve-fitting results of various $PVPh_{30}$-*b*-$PMMA_{70}$/PVP blends in terms of the fraction of hydrogen-bonded carbonyl of PVP and

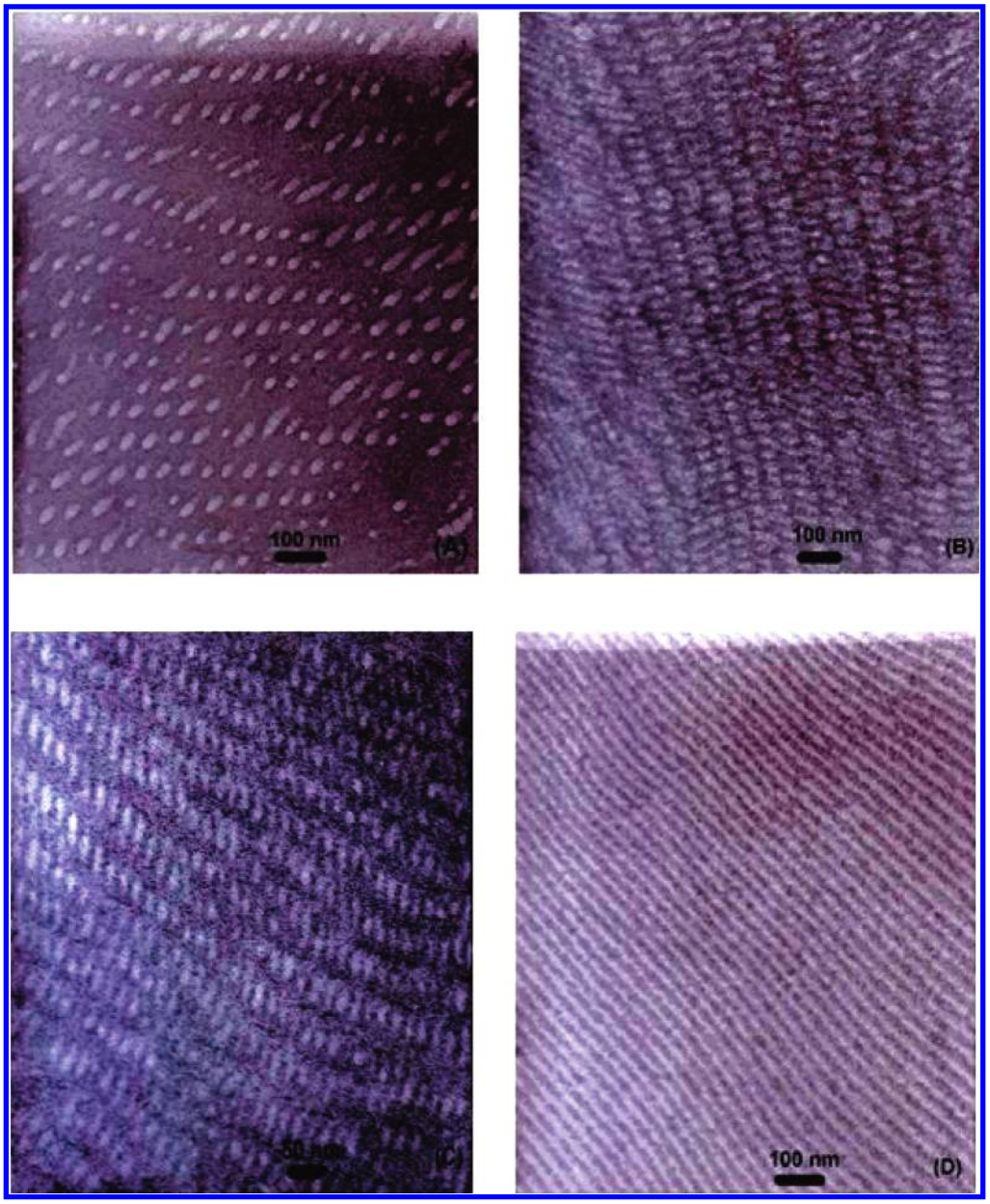

Figure 8. Transmission electron micrographs of the solution-cast films of (A) $PVPh_{55}$-*b*-$PMMA_{45}$/PVP = 60/40 wt %, (B) $PVPh_{30}$-*b*-$PMMA_{70}$/PVP = 60/40 wt %, (C) $PVPh_{40}$-*b*-$PMMA_{60}$/PVP = 80/20 wt %, and (D) $PVPh_{30}$-*b*-$PMMA_{70}$/PVP = 80/20 wt % blends stained with RuO_4. The dark region (matrix) corresponds to a mixed phase of −PVPh and PVP; the white region corresponds to −PMMA.

PMMA. It is clear that the PVPh hydroxyl is able to form hydrogen bonds with both PMMA and PVP when the PVP content is below 20 wt %. In other words, a fraction of these remaining free hydroxyl of PVPh is able to interact with the PMMA carbonyl. However, the PVPh hydroxyl only selectively interacts with PVP when the PVP content is above 20 wt %. These FTIR results are consistent with the prediction from the Painter−Coleman association model (PCAM). According to the PCAM,[38] the interassociation equilibrium constant of the PVPh/PVP blend (K_A = 6000) is significantly greater than that of the PVPh-*b*-PMMA copolymer (K_A = 47.1), implying that the hydrogen bond formation between PVP and PVPh predominates over that between PMMA and PVPh in these PVPh-*b*-PMMA/PVP blends.

Thermal Analyses. In general, differential scanning calorimetry (DSC) is one of the convenient methods to determine the miscibility in polymer blends. Figure 4 shows the conventional second run DSC thermograms of PVPh-*b*-PMMA/PVP blends in various compositions. The glass transition temperature (T_g) of the pure PVP is at 150 °C (0/100) while all PVPh-*b*-PMMA block copolymers have only one glass transition temperature because of the hydrogen bonds existed between PVPh and PMMA. $PVPh_{75}$-*b*-$PMMA_{25}$ is miscible with PVP over the whole composition range because the PVPh, as a rich content, can interact with both PVP and PMMA. On the other hand, systems of $PVPh_{55}$-*b*-$PMMA_{45}$/PVP, $PVPh_{40}$-*b*-$PMMA_{60}$/PVP, and $PVPh_{30}$-*b*-$PMMA_{70}$/PVP blends demonstrate two T_gs when the PVP contents are in the range of 20−60 wt % whereas one T_g with other PVP contents. The lower T_g in the range of 126−141 °C observed can be assigned as a signature of the PMMA domains, which are, presumably, phase separated from the mixed phase of miscible PVPh and PVP. In other words, the higher T_g can be considered as the T_g of hydrogen-bonded PVPh and PVP miscible phase. Figure 5 presents the T_g−composition curves for the PVPh-*b*-PMMA/PVP blends. For miscible blends and diblock copoly-

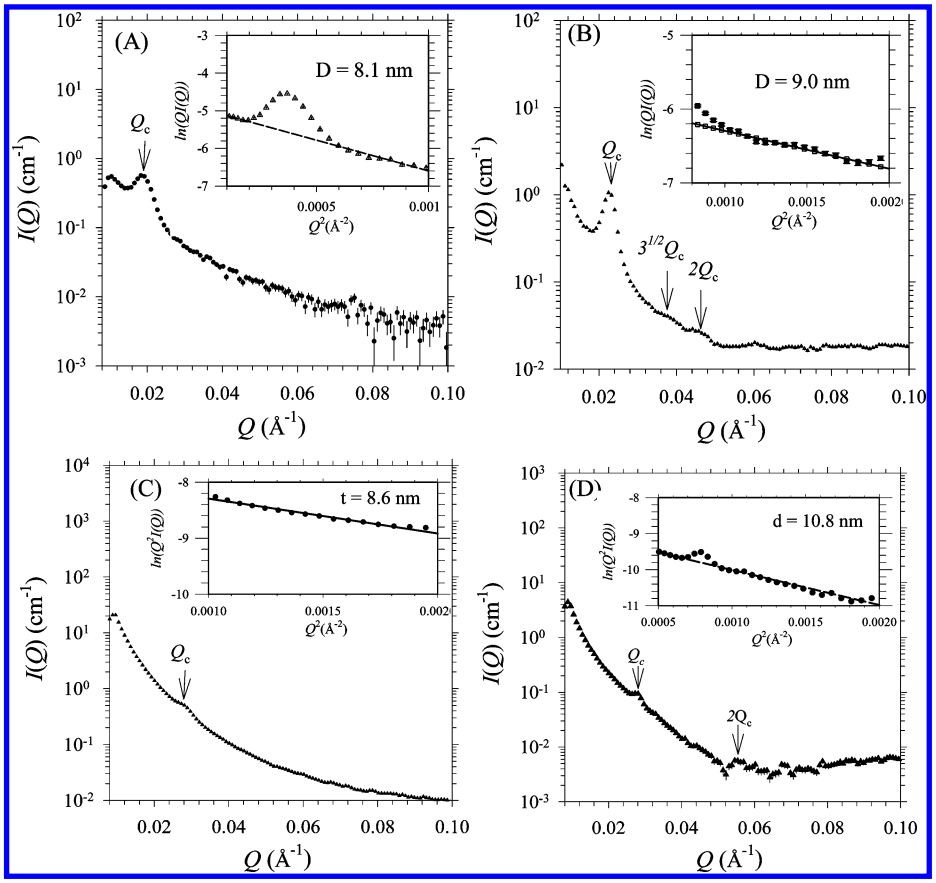

Figure 9. SAXS intensity profiles as a function of wave vector Q for (A) $PVPh_{55}$-*b*-$PMMA_{45}$/PVP = 60/40 wt %, (B) $PVPh_{30}$-*b*-$PMMA_{70}$/PVP = 60/40 wt %, (C) $PVPh_{40}$-*b*-$PMMA_{60}$/PVP = 80/20 wt %, and (D) $PVPh_{30}$-*b*-$PMMA_{70}$/PVP = 80/20 wt % blends at room temperature.

mers, T_g can be described by several empirical equations,[42−44] and the Kwei equation[44] is usually employed for systems with specific interactions

$$T_g = \frac{W_1 T_{g1} + kW_2 T_{g2}}{W_1 + kW_2} + qW_1W_2 \qquad (1)$$

where w_1 and w_2 are weight fractions of the compositions, T_{g1} and T_{g2} represent the corresponding glass transition temperatures, and k and q are fitting constants. Furthermore, $k = 1$ and $q = 140$ for PVPh/PVP blend have been obtained from the nonlinear least-squares fitting in our previous study.[29] Therefore, the same values of $k = 1$ and $q = 140$ are also adopted in this PVPh-*b*-PMMA/PVP system. As indicated in Figure 5, it fits well for those blends within the miscible ranges with relatively lower and higher PVP contents (<20 and >60 wt %). Within the immiscible range, 20−60 wt % PVP, phase separation occurs, and the Kwei equation is inapplicable as would be expected. At lower PVP contents (<20 wt %), the remnant PVPh not only interacts with PVP but also forms hydrogen bonds with the PMMA block of the PVPh-*b*-PMMA copolymers, as shown in Table 2. Therefore, blends of PVPh-*b*-PMMA/PVP at these compositions (<20 wt % PVP) are microscopically miscible. Upon further increasing of the PVP content (20−60 wt %), phase segregation to form the PMMA dominant domains occurs and induces two glass transition temperatures. Total miscibility on the macro- and microscales is expected at relatively higher PVP contents (e.g., 80 wt %), i.e., a mixed phase of miscible PVPh, PMMA, and PVP, because PVP is both miscible with PVPh[29] and PMMA.[45−47] Now, we consider that the T_g behavior is dictated by the PMMA content in these PVPh-*b*-PMMA/PVP blends. Table 3 summarizes the T_g behavior of these PVPh-*b*-PMMA/PVP blends; two T_gs phenomenon occurs only on those blends containing PMMA between 27 and 56 wt %. The PMMA contents within the range between 27 and 56 wt % give two T_gs. However, such T_g behavior is not linearly dependent on the PMMA content since the PVPh/PVP ratio also affects the T_g behavior of the miscible phase. Figure 6 displays the T_g behavior by changing the PVPh/PVP ratios, showing that the T_g behavior of PVPh/PVP mixed phase is increased rapidly at PVPh/PVP ratio <1, and the highest T_g is ca. 220 °C at around PVPh/PVP = 1/1. Further increase of the PVPh/PVP ratio above 1/1 does not result in further increase in T_g since the PVPh/PVP miscible phase is almost the same. Interestingly, T_gs of pure PVPh and pure PVP are 180 and 150 °C, while the T_g of resultant PVPh/PVP mixed phase is significantly higher than the average of corresponding homopolymers (ca. 40−70 °C) due to the strong hydrogen-bonding interaction existing between the hydroxyl group of PVPh and the carbonyl group of PVP. The T_g of the PVPh/PVP mixed phase in PVPh-*b*-PMMA/PVP blend (220 °C) is also higher than the corresponding PVPh/PVP homopolymer blend (T_g = 170−200 °C)[29,48] since the PVPh in block copolymer has less chain ends (one chain end connects PMMA) than PVPh homopolymer and thus results in smaller free volume and higher T_g. In addition, the observed T_g (135 °C) of the PMMA dominant phase is substantially higher than the T_g of the pure PMMA (105 °C) since this PMMA dominant phase probably contains miscible minor PVPh and PVP components which possess higher T_g and are able to form strong interactions (including hydrogen bonding) with PMMA.

The phase diagram of this PVPh-*b*-PMMA/PVP blending system is shown in Figure 7 based on DSC results listed in Table 3. As can been seen, there exists a closed-loop phase-separated region although PVPh-*b*-PMMA copolymers and

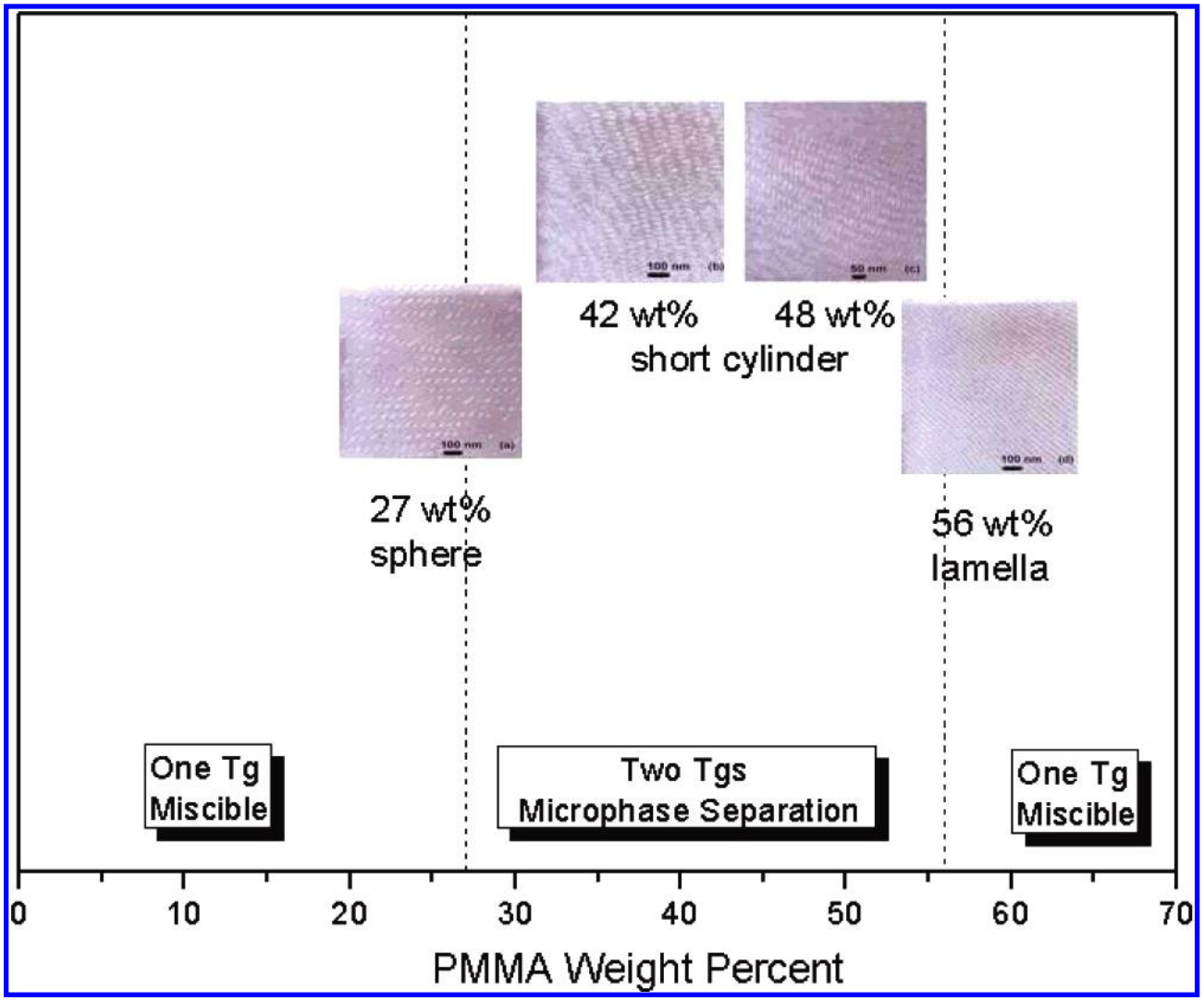

Figure 10. Phase diagram with various PMMA contents in PVPh-*b*-PMMA/PVP blends.

PVPh/PVP and PVP/PMMA blends are all miscible. When the PVP content is greater than the PVPh content, blends become miscible since the remnant PVP is able to interact with the PMMA phase through dipole−dipole interactions. On the other hand, the blends are also miscible when the PVP content is significantly lower than the PVPh content since the redundant PVPh is miscible with the PMMA phase through hydrogen-bonding interactions. As a result, the miscibility of these blends depends on the intriguing balance of the contents of PVP and PVPh.

TEM Analyses. TEM is used to investigate morphologies of these microphase-separated blends. Figure 8 illustrates the different types of morphologies observed by TEM. Thin films of different PVPh-*b*-PMMA/PVP blends with different compositions are stained with RuO_4 for 15−25 min. The PVPh chain is deeply stained, the PVP is lightly stained, and the PMMA is selectively unstained. At a lower PMMA fraction (27 wt %) in blend system, small PMMA microdomains are finely dispersed and confined within the matrix of miscible PVPh/PVP phase as shown in Figure 8A for $PVPh_{55}$-*b*-$PMMA_{45}$/PVP = 60/40. Most of these PMMA rich microdomains are nearly spherical, though some elongated ones are also present; hexagonal order is limited to local regions without a long-range ordering. The average microdomain radius measured by TEM micrographs is ca. 25 nm, and the distance between spheres is ca. 40 nm. Increasing the PMMA content to ca. 42−48 wt %, short PMMA cylinders dispersed within miscible phase of PVPh and PVP are obtained for $PVPh_{30}$-*b*-$PMMA_{70}$/PVP = 60/40 and $PVPh_{40}$-*b*-$PMMA_{60}$/PVP = 80/20 as shown in Figure 8B,C. Again, grains are small, and hexagonal order is localized. Further increasing the PMMA content to 56 wt %, the blend adopts a lamellar morphology as illustrated in Figure 8D for $PVPh_{30}$-*b*-$PMMA_{70}$/PVP = 80/20. Clearly, this lamellar structure shows highly long-range order pattern with lamellar period of ca. 30 nm. For a model AB diblock copolymer with strong degree of segregation χN, where χ is the Flory−Huggins segmental interaction parameter and N is the total number of segments in the copolymer chain, a lamellar phase is expected when both blocks occupy equal volume fractions. Grains of these morphologies shown in Figure 8 are not large, and the limited long-range ordering may be related to the disproportionate polydispersity between PVPh-*b*-PMMA and PVP as listed in Table 1. These block copolymers of PVPh-*b*-PMMA employed in this study are synthesized by anionic polymerization followed by sequential selective hydrolysis reaction. Therefore, the polydispersity index of PVPh-*b*-PMMA is significantly lower than that of PVP (1.92). The higher polydispersity of polymer matrix would influence the microphase separation and result in lower long-range order nanopattern.[49] The degree of phase segregation depends on the interaction parameter difference ($\Delta\chi$ or "ΔK in hydrogen-bonded system") between two polymer segments. As a result, the incorporation of PVP (solubility parameter: 11.0

Scheme 1. Schematic Illustration of the Phase Behavior of the PVPh-*b*-PMMA/PVP Blends

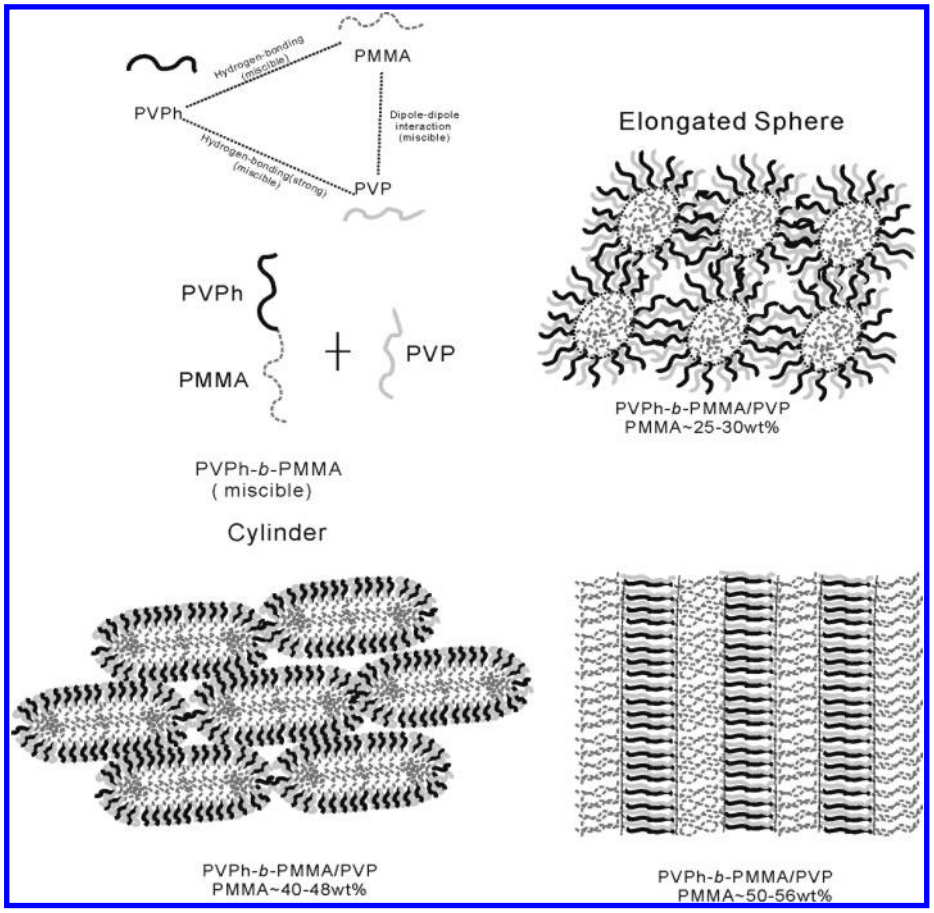

(cal/mL)$^{0.5}$) into PVPh-*b*-PMMA matrix (solubility parameter for PVPh: 10.6, PMMA: 9.1 (cal/mL)$^{0.5}$) would increase the interaction parameter difference between PVPh/PVP with PMMA phases. Therefore, the driving forces for this self-assembly structure come from not only the physical interaction difference but also different interassociation equilibrium constants from PVPh/PVP (K_A = 6000) and PVPh/PMMA (K_A = 47.1) phases. Although these two driving forces for self-assembly structures coexist in this copolymer/homopolymer, it is still insufficient to induce highly ordered structure except for PMMA content at ca. 50 wt %. When PMMA content is ca. 50 wt %, the nearly completed microphase separation results in a more ordered lamellar pattern as shown in Figure 8D. As a result, the DSC traces shown in Figure 4 display the highest T_g behavior for PVPh/PVP and PMMA phases, whereas that for the hydrogen-bonded carbonyl group of PMMA in the PVPh$_{30}$-*b*-PMMA$_{70}$/PVP = 80/20 blending has the lowest T_g as shown in Table 2. This result indicates that most hydroxyl groups of PVPh interact with the PVP for a mixed PVPh−PVP domain, which form an ordered lamellar morphology together with the phase-separated PMMA domains. However, with further increase of PVP content, the PVP is able to form dipole−dipole interaction with PMMA, thus reducing the degree of phase segregation even to a single phase.

SAXS Analyses. The microdomain structures of PVPh-*b*-PMMA/PVP system with different compositions are characterized by SAXS as displayed in Figure 9. The general features of the SXAS patterns observed are consistent with the corresponding TEM images in Figure 8; the TEM images are used as a basis in the SAXS data analysis. In Figure 9A, we analyze the SAXS data of the composition PVPh$_{55}$-*b*-PMMA$_{45}$/PVP = 60/40 using the rodlike form factor[50] as suggested by the TEM image (Figure 8A). The mean diameter of the cylinders D = 8.1 nm is extracted from the Kratky−Porod approximation shown in the inset of Figure 9A (dashed line), whereas the mean distance of the rods L = 34.2 nm is obtained from the scattering peak located Q_c = 0.0183 Å^{-1} using the Bragg diffraction ($L = 2\pi/Q_c$) approximation. For the composition PVPh$_{30}$-*b*-PMMA$_{70}$/PVP = 50/50, the scattering peaks in Figure 9B, with the ratio of peak positions of 1:$\sqrt{3}$:2, reveal an ordered phase of hexagonally packed cylinders (see Figure 8B). The first peak at Q_c = 0.0225 Å^{-1} corresponds to an intercylinder distance L of 32.2 nm, as determined from $L = \sqrt{4/3}2\pi/Q_c$.[51] Correspondingly, the inset of Figure 9B shows the Kratky−Porod approximation (dotted line) with a cylinder diameter of D = 9.0 nm. As the PMMA content increased further to PVPh$_{40}$-*b*-PMMA$_{60}$/PVP = 80/20, the PMMA form slablike domains, with the slab thickness t = 8.6 nm deduced from the Kratky−Porod approximation (dashed line in the inset of Figure 9C). The slablike domains form a short-range ordering, as suggested by the weak ordering peak at Q_c = 0.0281 Å^{-1}, which corresponds to a mean domain spacing of 22.3 nm ($= 2\pi/Q_c$). In the composition PVPh$_{30}$-*b*-PMMA$_{70}$/PVP = 50/50, a couple of SAXS peaks located at the positions of multiple Q_c = 0.028 09 Å^{-1} indicates a lamellar phase with a long period of 21.7 nm extracted from the first peak position ($2\pi/Q_c$). Furthermore, the inset of Figure 9D shows the Kratky−Porod approximation (dotted line) with a lamellar plate thickness of 10.8 nm, which agrees well with the TEM image observed (Figure 8D).

In the PVPh-*b*-PMMA/PVP system, all three components possess very close mass densities (1.19, 1.16, and 1.20 g/cm^3); therefore, small differences in the electron densities are expected among these three components (domains) since no crystalline

effect is involved in the phase separation. Therefore, we attribute the intensity differences of the four cases discussed in Figure 9 to the different degrees of phase separation. In Figure 9, we use the SAXS profiles at the absolute intensity scale for comparison in intensity. The larger scattering intensities for these compositions $PVPh_{40}$-*b*-$PMMA_{60}$/PVP(80:20 wt %) and $PVPh_{30}$-*b*-$PMMA_{70}$/PVP(80:20 wt %) shown in Figure 9C,D relative to those in Figure 9A,B are due to higher degrees of phase separation between PMMA and (PVPh + PVP), which is also supported by TEM images shown in Figure 8.

In the system studied, both the TEM and SAXS analyses clearly indicate the microphage separation under the intriguing balance of the hydrogen interactions among the three components of PVPh, PMMA, and PVP. As the increase of the PMMA content, PMMA can form ordered domains of hexagonally packed cylinders and a lamellar phase, in a limited region. As we have discussed earlier, polydisperse PVP in this blend system does not lead to perfect microphase separation, which is consistent with a low molecular weight polymer, when PVP interacts with PVPh through hydrogen bonding. A prolonged annealing at high-temperature (14 days at 150 °C) can significantly improve the long-range ordering in the system as shown in Figure 9; nevertheless, a highly long-range ordering with sharper and more multiple scattering peaks are increasingly difficult to obtain. In an earlier study, Sides and Fredrickson pointed out the effect of polydispersity on the introduction of trapped lattice disordering and defects in block copolymers,[52] which may be responsible for the long annealing time needed for a better ordering of the microdomains of the PVPh-*b*-PMMA/PVP blending system, having a substantial distribution of molecular weight of PVP.

In summary, Figure 10 shows the phase diagram with various PMMA contents in this PVPh-*b*-PMMA/PVP blend system. At PMMA contents <27 and >56 wt %, one single T_g is observed, and with PMMA contents between 27 and 56 wt %, two T_gs are observed, indicating phase separation in this region. Scheme 1 shows a schematic illustration of the possible inclusion and exclusion of the PMMA blocks in these immiscible PVPh-*b*-PMMA/PVP blends. The microphase-separated PMMA forms ordered phases with short rods (27 wt %), hexagonally packed cylinders (42−48 wt %), to lamella (56 wt % PMMA). However, we do not find the inverse phase morphologies by increasing PMMA contents as shown in typical diblock phase diagram.[53] These miscible diblock copolymers unusually formed typical self-assembly structures through the mediation of the subtle balance between the hydrogen-bonding interactions of PVPh/PVP and PVPh/PMMA blends. The positive result shown in this study shed lights on a promising direction in using monodisperse homopolymer to induce well-ordered microdomain structure from blending with a miscible diblock copolymer system through similar hydrogen-bonding interactions.

Conclusions

DSC, FTIR, TEM, and SAXS techniques have been employed to investigate in detail the miscibility, phase behavior, and hydrogen-bonding interaction mechanism of novel A−B/C type polymer blends composed of miscible PVPh-*b*-PMMA and PVP. FTIR spectra provide evidence that the PVP carbonyl groups are significantly stronger hydrogen bond acceptors than are the PMMA carbonyl groups. Moreover, DSC results demonstrate that phase transition occurred in this A−B/C blend system which A−B diblock copolymer is original miscible; however, the microphase separation would occur with the increase of PVP content at ca. 20−60 wt %. TEM imaging and SAXS indicate that different compositions of the PVPh-*b*-PMMA/PVP blends induce different microphase separation structures through the mediation of hydrogen-bonding interactions. The blends become homogeneous (miscible) again at a higher PVP content (>80 wt %) through the dipole−dipole interaction between PMMA and PVP. In conclusion, the phase behavior and miscibility the of this A−B/C blend system are influenced by two main factors: first, the difference in the hydrogen-bonding strengths between the PVPh/PVP and PVPh/PMMA, which appears to be the major factor; second, the content and polydispersity of PVP.

Acknowledgment. This work was supported financially by the National Science Council of the R.O.C. under Contracts NSC-96-2120-M-009-009 and NSC-96-2218-E-110-008 and Ministry of Education "Aim for the top University" (MOEATU) program. The SAXS experiments were conducted at beamline BL17B3 at the National Synchrotron Radiation Research Center (NSRRC), Taiwan.

References and Notes

(1) Hashimoto, T.; Tanaka, H.; Hasegawa, H. *Macromolecules* **1990**, *23*, 4378.
(2) Tanaka, T.; Hasegawa, H.; Hashimoto, T. *Macromolecules* **1991**, *24*, 240.
(3) Bendejacq, D.; Ponsinet, V.; Joanicot, M. *Macromolecules* **2002**, *35*, 6645.
(4) Holoubek, J.; Baldrian, J.; Lednicky, F.; Malkova, S.; Lal, J. *Macromol. Chem. Phys.* **2006**, *207*, 1834.
(5) Tucker, P. S.; Barlow, J. W.; Paul, D. R. *Macromolecules* **1988**, *21*, 2794.
(6) Tucker, P. S.; Paul, D. R. *Macromolecules* **1988**, *21*, 2801.
(7) Lowenhaupt, B.; Steurer, A.; Hellmann, G. P. *Polymer* **1991**, *32*, 1065.
(8) Lowenhaupt, B.; Steurer, A.; Hellmann, G. P.; Gallot, Y. *Macromolecules* **1994**, *27*, 908.
(9) Han, Y. K.; Pearce, E. M.; Kwei, T. K. *Macromolecules* **2000**, *33*, 1321.
(10) Zhao, J. Q.; Pearce, E. M.; Kwei, T. K. *Macromolecules* **1997**, *30*, 7119.
(11) Jiang, M.; Xie, H. K. *Prog. Polym. Sci.* **1991**, *16*, 977.
(12) Jiang, M.; Huang, T.; Xie, J. *Macromol. Chem. Phys.* **1995**, *196*, 787.
(13) Jiang, M.; Huang, T.; Xie, J. *Macromol. Chem. Phys.* **1995**, *196*, 803.
(14) Zoelen, W. V.; Ekenstein, G. A. V.; Ikkala, O.; Brinke, G. T. *Macromolecules* **2006**, *39*, 6574.
(15) Lee, J. H.; Balsara, N. P.; Chakraborty, A. K.; Krishnamoorti, R.; Hammouda, B. *Macromolecules* **2002**, *35*, 7748.
(16) Akaba, M.; Nojima, S. *Polym. J.* **2006**, *38*, 559.
(17) Huang, Y. M.; Liu, H. L.; Hu, Y. *Macromol. Theory Simul.* **2006**, *15*, 321.
(18) Huang, Y. Y.; Chen, H. L.; Hashimoto, T. *Macromolecules* **2003**, *36*, 764.
(19) Likhman, A. E.; Semenov, A. N. *Macromolecules* **1997**, *30*, 7273.
(20) Huang, Y. Y.; Hsu, J. Y.; Chen, H. L.; Hashimoto, T. *Macromolecules* **2007**, *40*, 3700.
(21) Matsushita, Y. *Macromolecules* **2007**, *40*, 771.
(22) Stoykvich, M. P.; Edwards, E. W.; Solak, H. H. *Phys. Rev. Lett.* **2006**, *97*, 147802.
(23) Jinnai, H.; Hasegawa, H.; Nishikawa, Y.; Sevink, G. J. A.; Braunfeld, M. B.; Agard, D. A.; Spontak, R. J. *Macromol. Rapid Commun.* **2006**, *27*, 1424.
(24) Lee, J. H.; Balsara, N. P.; Chakraborty, A. K.; Krishnamoorti, R.; Hammouda, B. *Macromolecules* **2002**, *35*, 7748.
(25) Vaidya, N. Y.; Han, C. D. *Polymer* **2002**, *43*, 3047.
(26) Huang, P.; Zhu, L.; Cheng, S. Z. D.; Ge, Q.; Quirk, R. P.; Thomas, E. L.; Lotz, B.; Hsiao, B. S.; Liu, L. Z.; Yeh, F. J. *Macromolecules* **2001**, *34*, 6649.
(27) Vavasour, J. D.; Whitmore, M. D. *Macromolecules* **2001**, *34*, 3471.
(28) Maurer, W. W.; Bates, F. S.; Lodge, T. P. *J. Chem. Phys.* **1998**, *108*, 2989.
(29) Kuo, S. W.; Chang, F. C. *Macromolecules* **2001**, *34*, 5224.
(30) Kuo, S. W.; Chang, F. C. *Polymer* **2003**, *44*, 3021.
(31) Xu, H.; Kuo, S. W.; Lee, J. S.; Chang, F. C. *Polymer* **2002**, *43*, 5117.
(32) Chen, D.; Jiang, M. *Acc. Chem. Res.* **2005**, *38*, 494.
(33) Coleman, M. M.; Painter, P. C. *Prog. Polym. Sci.* **1995**, *20*, 1.

(34) Manestrel, C. L.; Bhagwagar, D. E.; Painter, P. C.; Coleman, M. M.; Graf, J. F. *Macromolecules* **1992**, *25*, 7101.
(35) Jo, W. H.; Kwon, Y. K.; Kwon, I. H. *Macromolecules* **1991**, *24*, 4708.
(36) Kuo, S. W.; Lin, C. L.; Chang, F. C. *Macromolecules* **2002**, *35*, 278.
(37) Lin, C. L.; Chen, W. C.; Liao, C. S.; Su, Y. C.; Huang, C. F.; Kuo, S. W.; Chang, F. C. *Macromolecules* **2005**, *38*, 6435.
(38) Coleman, M. M.; Graf, J. F.; Painter, P. C. *Specific Interactions and the Miscibility of Polymer Blends*; Technomic Publishing: Lancaster, PA, 1991.
(39) Hu, Y.; Motzer, H. R.; Etxeberria, A. M.; Fernadez-Berridi, M. J.; Iruin, J. J.; Painter, P. C.; Coleman, M. M. *Macromol. Chem. Phys.* **2000**, *201*, 705.
(40) Lai, Y. H.; Sun, Y. S.; Jeng, U.; Lin, J. M.; Lin, T. L.; Sheu. H. S.; Chuang, W. T.; Huang, Y. S.; Hsu, C. H.; Lee, M. T.; Lee, H. Y.; Liang, K. S.; Gabriel, A.; Koch, M. H. J. *J. Appl. Crystallogr.* **2006**, *39*, 871.
(41) Moskala, E. J.; Varnell, D. F.; Coleman, M. M. *Polymer* **1985**, *26*, 228.
(42) Fox, T. G. *J. Appl. Bull. Am. Phys. Soc.* **1956**, *1*, 123.
(43) Gordon, M.; Taylor, J. S. *J. Appl. Chem.* **1952**, *2*, 493.
(44) Kwei, T. K. *J. Polym. Sci., Polym. Lett. Ed.* **1984**, *22*, 307.
(45) Hsu, W. P. *J. Appl. Polym. Sci.* **2001**, *81*, 3190.
(46) da Silva, E. P.; Tavares, M. I. B. *Polym. Bull. (Berlin)* **1998**, *41*, 307.
(47) Lee, H. F.; Kuo, S. W.; Huang, C. F.; Lu, J. S.; Chan, S. C.; Wang, C. F.; Chang, F. C. *Macromolecules* **2006**, *39*, 5458.
(48) Prinos, A.; Pompros, A.; Panayiotou, C. *Polymer* **1998**, *14*, 3011.
(49) Chu, B.; Hsiao, B. S. *Chem. Rev.* **2001**, *101*, 1727.
(50) Lin, T. L.; Jeng, U.; Tsao, C. S.; Liu, W. J.; Canteenwala, T.; Chiang, L. Y. *J. Phys. Chem. B* **2004**, *108*, 14884.
(51) Yeh, S. W.; Wei, K. H.; Sun, Y. S.; Jeng, U. S.; Liang, K. S. *Macromolecules* **2003**, *36*, 7903.
(52) Sides, S. W.; Fredrickson, G. H. *J. Chem. Phys.* **2004**, *121*, 4974.
(53) Foster, S.; Plantenberg, T. *Angew. Chem., Int. Ed.* **2002**, *41*, 688.

MA7021925